THE ASTROPHYSICAL JOURNAL, 932:104 (6pp), 2022 June 20
© 2022. The Author(s). Published by the American Astronomical Society.

OPEN ACCESS

https://doi.org/10.3847/1538-4357/ac6fd4

Hard X-Ray Emission in Centaurus A

B. Rani[1,2,3] , S. A. Mundo[4] , R. Mushotzky[4] , A. Y. Lien[5], M. A. Gurwell[6] , and J. Y. Kim[7,8]

[1] Korea Astronomy and Space Science Institute, 776 Daedeokdae-ro, Yuseong-gu, Daejeon 30455, Republic of Korea; binduphysics@gmail.com
[2] University of Science and Technology, Korea, 217 Gajeong-ro, Yuseong-gu, Daejeon 34113, Republic of Korea
[3] Department of Physics, American University, Washington, DC 20016, USA
[4] Department of Astronomy, University of Maryland, College Park, MD 20742, USA
[5] University of Tampa, Department of Chemistry, Biochemistry, and Physics, 401 W. Kennedy Blvd, Tampa, FL 33606, USA
[6] Center for Astrophysics—Harvard Smithsonian, 60 Garden Street, Cambridge, MA 02138 USA
[7] Department of Astronomy and Atmospheric Sciences, Kyungpook National University, Daegu 702-701, Republic of Korea
[8] Max-Planck-Institut für Radioastronomie, Auf dem Hügel 69, D-53121 Bonn, Germany
Received 2022 April 26; revised 2022 May 10; accepted 2022 May 11; published 2022 June 21

Abstract

We use 13 yr of Swift/BAT observations to probe the nature and origin of the hard X-ray (14–195 KeV) emission in Centaurus A. Since the beginning of the Swift operation in 2004, significant X-ray variability in the 14–195 KeV band has been detected, with mild changes in the source spectrum. Spectral variations became more eminent after 2013, following a softer-when-brighter trend. Using the power spectral density (PSD) method, we find that the observed hard X-ray photon flux variations are consistent with a red-noise process of slope, −1.3, with no evidence for a break in the PSD. We find a significant correlation between the hard X-ray and 230 GHz radio flux variations, with no time delay longer than 30 days. The temporal and spectral analysis confirms that the X-ray emission generated by the accretion in the ADAF model is sub-dominant as compared with the emission arising from that produced by the inner regions of the radio jet.

Unified Astronomy Thesaurus concepts: X-ray active galactic nuclei (2035); Active galactic nuclei (16); Radio active galactic nuclei (2134)

1. Introduction

The X-ray-emitting sites in Active Galactic Nuclei (AGNs) are not well understood. X-rays could either originate in the immediate vicinity of the central black hole (disk/corona) or further out in the jets. Some of these X-rays penetrate into the disk, where they are reprocessed to produce the "reflection" spectrum that includes the Fe Kα line (Lohfink et al. 2013; Hinkle & Mushotzky 2021). The geometry of the disk/corona is an active area of research. A detailed understanding of the disk/corona/jet contribution to the observed X-ray emission is a critical element for unraveling how the central engine of an AGN operates and feeds the jet. In this paper, we investigate the origin of the hard X-ray emission in a nearby AGN, Centaurus A (hereafter, Cen A), using the observed variations in the X-ray and radio regimes.

At a distance of $d \simeq 3.8$ Mpc (Harris et al. 2010), Cen A is the closest AGN hosting a supermassive black hole of $\sim 5 \times 10^7 M_\odot$ (Neumayer 2010). From the radio morphology of the lobes, Cen A is classified as being Fanaroff–Riley type I (Fanaroff & Riley 1974). In fact, the Cen A jet has been detected and extensively studied across the whole electromagnetic spectrum, from radio to γ-rays (Hardcastle et al. 2003; Worrall et al. 2008; Abdo et al. 2010; Müller et al. 2014; Wykes et al. 2015; Janssen et al. 2021). In 2004, the source was first detected at TeV energies by the High Energy Stereoscopic System (Aharonian et al. 2009), and later by the Fermi Large Area Telescope (Fermi/LAT) at GeV energies (Abdo et al. 2010). Spatial extension of the γ-ray emission has been detected at both GeV (Abdo et al. 2010) and TeV energies

(HESS Collaboration et al. 2020), the physical origin of which remains unclear.

The X-ray (0.1–7 KeV) morphology of Cen A consists of a central bright AGN and a faint jet component surrounded by diffuse emission (Kraft et al. 2002). The source has a complex X-ray spectrum, comprising a soft (0.1–2 KeV) thermal plasma, a power-law continuum, and strong absorption of the power-law continuum. The location and structure of the absorbing material is still under debate (e.g., Evans et al. 2004; Markowitz et al. 2007; Fukazawa et al. 2011). The hard X-ray spectrum of the source can be well described by an absorbed power-law or thermal Comptonization spectrum with an Fe Kα line, with no evidence for a high-energy exponential rollover (Fürst et al. 2016). The detection of a weak reflection component has been reported (Fukazawa et al. 2011; Burke et al. 2014), but recent analysis has placed a very tight upper limit on the presence of such a reflection component (Beckmann et al. 2011; Rothschild et al. 2011; Fürst et al. 2016). Small changes in the hard X-ray power-law continuum photon index have been reported over past decades (Baity et al. 1981; Rothschild et al. 2011; Fürst et al. 2016), with the slope being bounded between 1.6 and 1.85. This range of indices is consistent with what is found for Seyfert galaxies.

While the continuum flux is strongly variable over time, the flux of the iron line has remained stable, indicating the strong variability of the equivalent width of the iron line (Rothschild et al. 2006). Even a joint spectral analysis, using truly simultaneous XMM-Newton and NuSTAR data, could not determine the physical origin of the hard X-ray emission in the source (Fürst et al. 2016). The study found no significant contribution from the hot interstellar medium, the outer jet, or off-nuclear point sources to the hard X-ray spectrum. The lack of reflection rules out the standard Seyfert-like geometry of the source of the hard X-rays and reprocessing material.

Original content from this work may be used under the terms of the Creative Commons Attribution 4.0 licence. Any further distribution of this work must maintain attribution to the author(s) and the title of the work, journal citation and DOI.

1

Comptonization in an advection-dominated accretion flow (ADAF) or at the base of the inner jet, or a combination of the two, have been proposed as possible mechanisms for the hard X-ray emission in the source (Fürst et al. 2016). We present here a comprehensive analysis of the observed variations in the X-ray and radio regions to better understand the nature and origin of the hard X-ray emission. The paper is structured as follows. In Section 2, we present the data analysis and results. The results are discussed in Section 3, and summarized in Section 4.

2. Data Analysis and Results

2.1. X-Rays

We investigated the X-ray flux and spectral variations of the source using data from the Neil Gehrels Swift Observatory/ Burst Alert Telescope (Swift/BAT) 157-month Hard X-Ray Survey.[9] When it is in survey mode (i.e., not specifically targeting a gamma-ray burst), BAT continuously scans the sky with a time resolution as fine as 64 s (Krimm et al. 2013). The monthly averaged light curves and spectra of sources in the hard X-ray (14–195 KeV) sky are publicly available online. In addition to the 8-band (14–20, 20–24, 24–35, 35–50, 50–75, 75–100, 100–150, and 150–195~KeV) monthly averaged data, the website also provides 8-band snapshot light curves, starting from 2005. The snapshot light curves are extremely useful for exploring the short-timescale variability. The snapshot data is binned to generate 10 day binned light curves in the different energy bands, then a total count rate for the 14–100 KeV energy range. While binning, we flagged the low-exposure (<1 day) epochs to reduce systematic errors. Given the low signal-to-noise ratios (S/Ns) in bands 7 and 8, we discarded the 100–195 KeV energy band data.

Figure 1(a) shows the monthly averaged hard X-ray (14–195 KeV) light curve from 2004 December to 2017 December (blue circles). Prominent flux variations were detected in the source during this period. The red squares show the 10 day binned light curves in the 14–100 KeV energy range. The count rates are scaled by a factor of 15 for visualization only. Given the high S/N of the monthly binned data, the intensity variations can be studied in different energy bands. Photon flux light curves in different energy bands (14–20, 20–24, 24–35, 35–50, 50–75, 75–100, and 100–150 KeV) are plotted in Figure 1(b). Band 8 (150–195 KeV) is not included in the plot because of its low S/N. Similar variations are seen across multiple bands. The variability is less pronounced in the higher-energy bands (>75 KeV) because of the low S/N.

The monthly (blue circles) and bimonthly (red squares) averaged hard X-ray photon index curve are illustrated in Figure 1(c). Despite the significant flux variations in the X-ray bands, the changes in the photon index were small but significant ($\Gamma \sim 1.7$–1.9) until the end of 2012. The spectral variations were more pronounced afterward. The steepening of the spectrum was observed until December 2013, reaching $\Gamma \sim 2.0$. Later, spectral hardening occurred until February 2015 ($\Gamma \sim 1.7$). The spectra have softened back to the average value ($\Gamma \sim 1.8$) over recent years, with some mild variations. In short, the hard X-ray spectra follow a steeper-when-brighter trend. This trend is evident in the index versus photon flux plot (the

top panel of Figure 2). A linear Pearson correlation test is used to quantify the correlation; we obtained r_P(correlation coefficient) = 0.43 at the 99.8% confidence level for the bimonthly binned data, and $r_P = 0.16$ at the 90% confidence level for the monthly binned data.

We further investigate the spectral variability by analyzing hardness ratio (HR) time series. The monthly averaged data is used to calculate the time series in the following three energy bands: the low or L-channel, from 14 to 24 keV; the medium or M-channel, from 24 to 50 keV; and the high or H-channel, from 50 to 150 keV. We rebin the hard X-ray spectrum in this way in order to maximize the S/N. (We exclude the 150–195 keV data due to the low S/N.) We then calculate the HR values using these three channels, and confirm through a chi-squared test that the HR time series show statistically significant variability (p-value <0.05). The ratios of the time series in the different channels are then plotted against each other to produce an "HR plane" (Figure 2, black circles), and are used to investigate the nature of the spectral variability in the source. A visual correlation can be seen between the HL and ML ratios. A linear Pearson correlation analysis confirms the correlation between the two. Formally, the Pearson correlation coefficient equals 0.71 at the >99.99% confidence level. We further tested the spectral variations using simulations. The spectral simulations, using different power-law slopes, were performed using the "fakeit" command on Xspec (Arnaud 1996). The simulations were based on the simple "pegpwrlw" model, with Γ in the range of 1 to 3 (the typical photon indices of AGNs in the Swift/BAT catalog). We then calculated the HRs from the fake spectra (shown as the colored stars in Figure 2). The details of the simulations can be found in S. A. Mundo et al. (2022, in preparation). The simulated points agree with the data, suggesting that the changing spectrum can be well described as a simple power law with a varying photon index over monthly timescales, spanning the range 1.6–2.

The nature of the hard X-ray variability in the source is explored using the power spectrum density (PSD; Vaughan et al. 2003) analysis method. Both the monthly averaged 14–195 KeV (data A) and 10 day binned 14–100 KeV (data B) light curves are used for the PSD analysis. As a first step, we calculate the raw PSDs and the squared modulus of the discrete Fourier transform. The raw PSDs are then logarithmically binned to extract the slope of the underlying power spectrum, $P(f) \propto f^{\alpha}$ (for details, readers are referred to Chidiac et al. 2016). The Poisson noise level in the PSD is calculated following Vaughan et al. (2003). The PSD analysis results are shown in Figure 3, where the cyan and brown steps are the raw PSDs for data A and data B, respectively, and the blue circles and red squares are their logarithmic binned values; the errors mark the scatter of the raw PSD points. The best-fit power-law slope for data A is $-(1.36 \pm 0.16)$ and for data B it is $-(1.29 \pm 0.11)$. A combined power-law fit gives, $\alpha = -(1.27 \pm 0.13)$ (the black dashed line in Figure 3). We do not find any evidence of a break in the PSD, as is sometimes seen in the 2–10 KeV PSD of Seyfert galaxies (Vaughan et al. 2005). A similar value for the PSD slope was reported by Shimizu & Mushotzky (2013), using 58 months of Swift/BAT data, and comparable slopes have been seen in the PSDs of beamed AGNs (Chidiac et al. 2016; Algaba et al. 2018) as well. This implies that the hard X-ray variability of the source can be characterized simply as a red-noise process. Since there is no excess power at any frequency in the given time range, the PSD
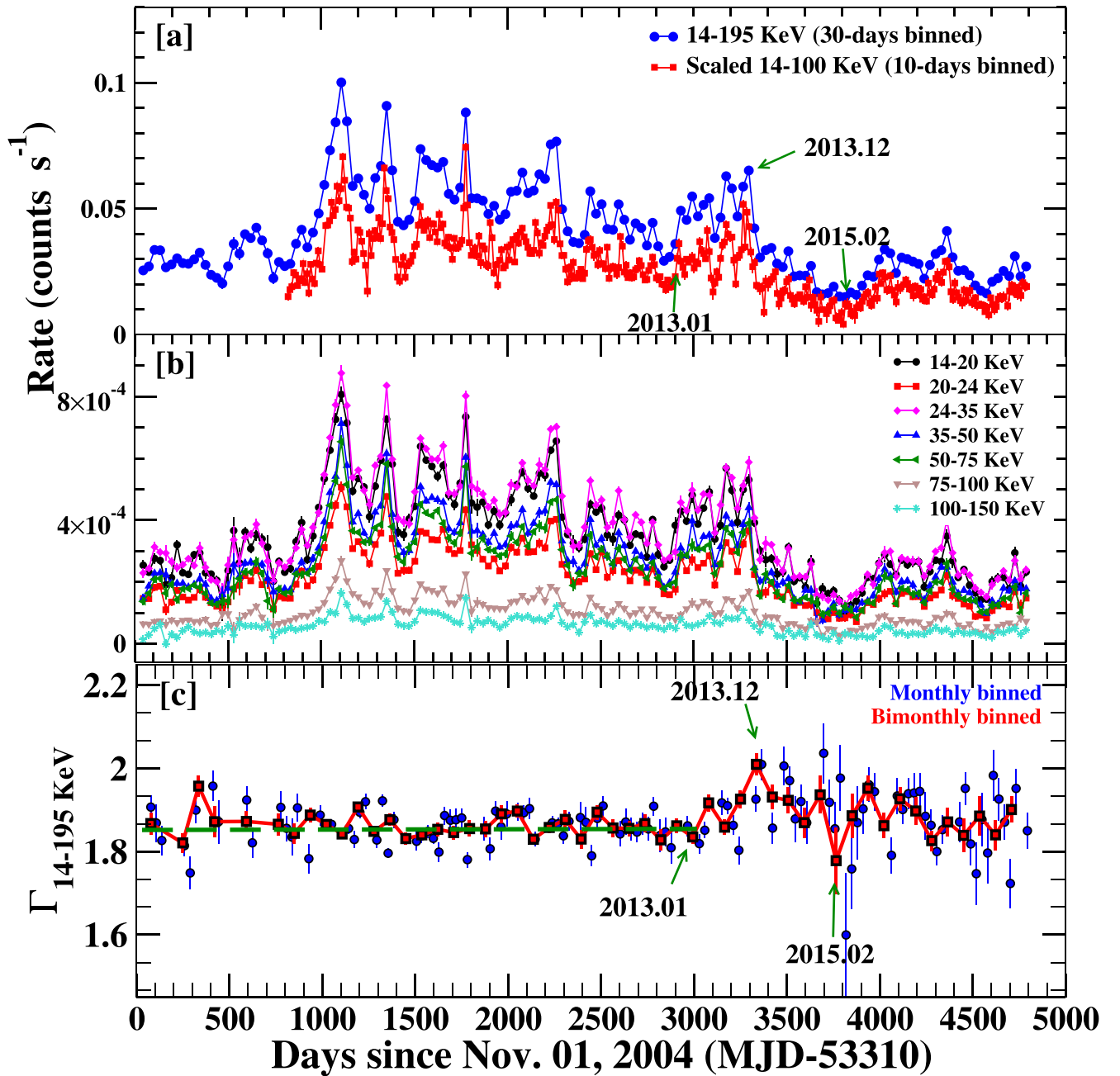

Figure 1. Photon flux and spectral variations observed in Cen A since 2004 November. Panel (a): monthly averaged 14–195 KeV (blue circles) and 10 day binned 14–100 KeV (red squares) light curves. The 10 day binned data is scaled by a factor of 15. Panel (b): monthly averaged light curves in the different energy bins. Panel (c): hard X-ray photon index variations observed at the source. The green arrows mark the prominent spectral variability phases of the source (see Section 2.1 for more details).

analysis rules out the presence of periodic variations in the source.

2.2. Radio Submillimeter Array

We used the 230 GHz data provided by the Submillimeter Array Observer Center[10] database (Gurwell et al. 2007) to investigate the flux variations in the radio regime. Figure 4 (red squares) shows the flux density variations observed in the source since 2005 July. The radio flux variations are superimposed on top of a constant flux level of about 6 Jy

(the dashed line), and this could be related to the extended jet emission (see Section 3.1 for details). Compared to X-rays (blue circles), the radio data is sparsely sampled, especially in the beginning (segment T1). Some similarities in the long-term decay trends can be seen in the two data sets, over segment T2, and the flux variations are quite similar afterward (segment T3).

2.3. Cross-correlation

The apparent correlation among the X-ray and radio data sets was quantified using the discrete correlation function (DCF; Edelson & Krolik 1988) method, and the significance of the correlation was tested via simulations, as discussed in Section
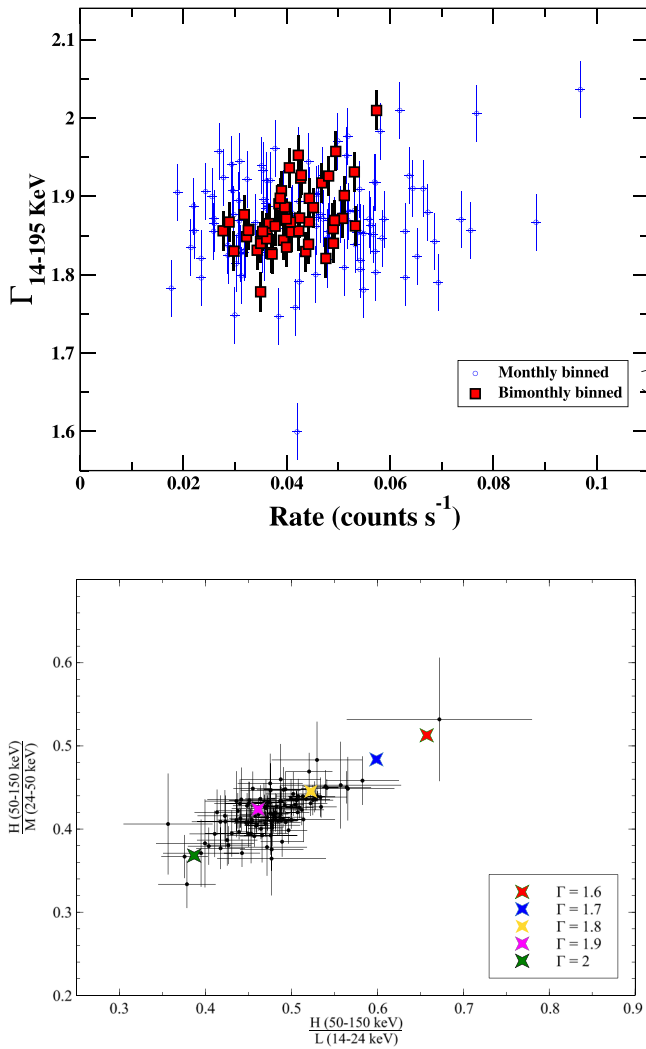
---

[10] http://sma1.sma.hawaii.edu/callist/callist.html

Figure 2. Top: photon index vs. photon flux plot. Bottom: spectral variability of Cen A in the HR plane. The black circles are the estimated HRs in the different energy channels, while the colored stars mark the simulated points.
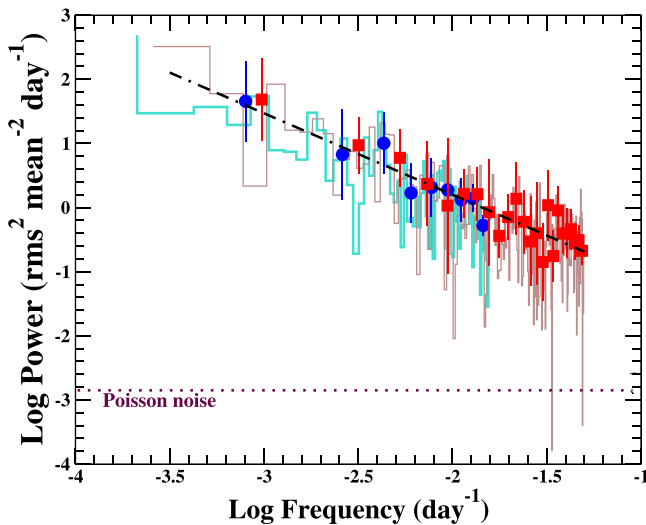

Figure 3. Raw PSDs of the monthly (in cyan) and 10 day (in brown) binned X-ray light curves. The dotted line marks the estimated Poisson noise level. The blue circles and red squares are the logarithmically binned PSDs for the monthly and 10 day binned data sets, respectively. The black dashed line is the best-fit power law with a slope = 1.27 ± 0.13.

A of Rani et al. (2014). The DCF results are presented in the right panel of Figure 4. The monthly binned DCF points are in blue, while the red curves show the 95% confidence levels. The DCF analysis of the two data sets shows a peak above the 95% confidence level at 0 days. This implies that the flux variations in the X-ray and radio regimes are well correlated, with no time lag. Since the X-ray data is sampled on a monthly basis, a time delay shorter than 30 days cannot be tested. The correlation analysis therefore suggests that the hard X-ray and radio emission regions are cospatial. This agrees with the tight correlation found between the parsec-scale radio luminosity and the X-ray luminosity of BAT-detected Seyfert galaxies (Baek et al. 2019). Radio and X-ray (especially soft X-ray) correlations have also been reported in several other Seyfert galaxies (Chatterjee et al. 2009, 2011; Marscher et al. 2018) and explicitly used to probe the disk-jet connection in AGNs.

3. Discussion

Detailed spectral analysis (Fürst et al. 2016) suggests that the hard-X-ray-emitting site is close to the central engine, but it could not disentangle the ADAF and the jet contribution. The multiwavelength variability analysis presented here allows us to do so. Using 13 yr of Swift/BAT and 230 GHz data, we performed a detailed temporal and correlation analysis, which revealed the following. Prominent flux variations had been observed in the source since 2004, but the spectral changes were rather moderate until 2012. Significant spectral variations were observed afterward, following a softer-when-brighter trend. The hard X-ray flux variability of the source is consistent with red-noise processes, with a slope ~ -1.3. Variations in the hard X-ray and 230 GHz radio data are correlated, with no time lag. In the following subsections, we discuss the origin of the hard X-ray emission in the context of the ADAF and jet models.

3.1. Nature of X-Ray Variability

There have been many PSD studies of AGNs, characterizing the PSD slopes, breaks, and their relation to the physical properties of the central engine. Breaks are a common feature in the PSDs of Seyfert galaxies (Markowitz et al. 2003; Papadakis 2004; Done & Gierliński 2005). These studies, however, are focused on the soft X-ray emission (<10 KeV), and the hard X-ray variability studies differ from this picture (Shimizu & Mushotzky 2013). The hard X-ray PSD of Cen A is well-fitted using a slope of -1.3, with no evidence of a break. If we scale the breaks seen in the X-ray PSDs by the mass, as in McHardy et al. (2004), the predicted break timescale is higher than 20 days ($\log 10$ (Frequency) > -1.3 day^{-1}), and is thus not sensed by the BAT data. It is important to note that, unlike Seyfert galaxies, Cen A is a low-luminosity radio-loud AGN, and, as our study suggests, the PSD slope is comparable to those seen in the PSDs of beamed AGNs.

Except for the power-law slope ($\Gamma = 1.6–2.0$), the X-ray spectrum of the source (with no reflection and very high cutoff energy; Fürst et al. 2016) differs from that of Seyfert galaxies. Since the power-law slopes from the jet and from the thermal Comptonization are very similar, the spectral slope cannot be used as a means of distinction between the two. However, the differences in the source spectra and the temporal variations favor the nature of the X-ray emission in Cen A being similar to that of beamed AGNs.
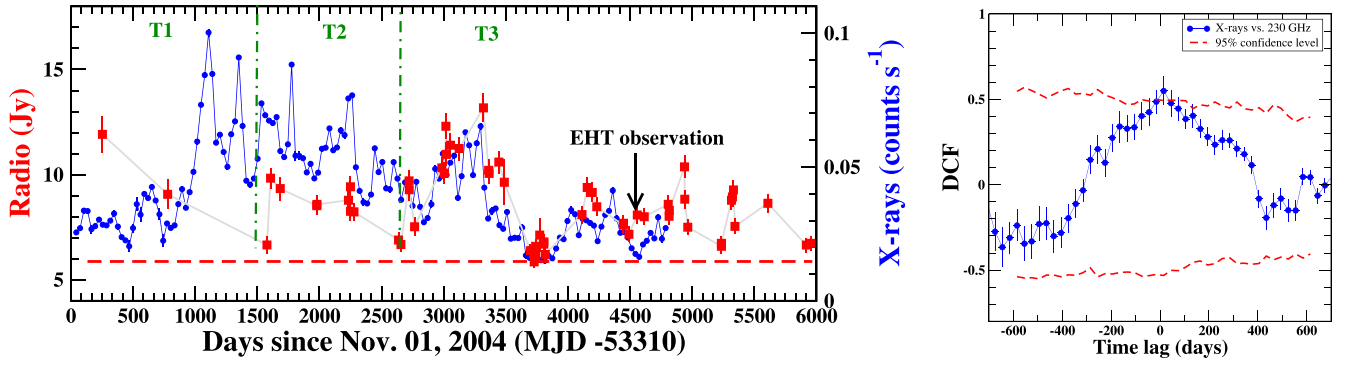
Figure 4. Left panel: 230 GHz flux density light curve (red squares) superimposed on top of the 14–150 KeV light curve (blue circles). Right panel: cross-correlation analysis results—the DCF curve is in blue, while the red dashed lines mark the 95% confidence level.

3.2. Nature of 230 GHz Variability

The radio variations comprise two components: quiescent and variable. As shown in Figure 4, even at 230 GHz, we have about a 6 Jy contribution from the extended jet region. Earlier studies found a contribution of about 7 Jy from the extended jet emission in the total flux density of the source (Israel et al. 2008). Since Cen A has a complex extended jet structure, the location of the variable component has remained unclear. Using continuum observations in the millimeter and submillimeter regime, Israel et al. (2008) investigated the flux and spectral variability of the source, and reported that most (if not all) of the variations are from the milliarcsecond core. On microarcsecond scales, the Event Horizon Telescope (EHT) discovered a completely different picture of the core (Janssen et al. 2021). The core of the source is opaque at 230 GHz, and the turnover frequency is at $\sim$ THz frequencies. The source has a flux density of $\sim$2 Jy, with an edge-brightened jet. It is quite probable that the flux density of either the core or the two lanes varies, but multiple observations are required to confirm this. The radio luminosity of the source, measured by EHT, is 7.5×10^{39} erg s^{-1}. However, EHT observed the source when it was not in its brightest phase (see Figure 4). After subtracting the quiescent flux (6 Jy) from the total flux, the peak flux of the variable component is $\sim$7 Jy, which corresponds to 2.6×10^{40} erg s^{-1}.

3.3. ADAF versus Jet Models

In the ADAF model, the radio emission occurs because of cyclo-synchrotron radiation from hot electrons in the equipartition magnetic field; it should be isotropic. In the absence of a radio jet, the expected radio luminosity is roughly proportional to the mass of the central black hole and its accretion rate (Mahadevan 1997; Yi & Boughn 1999), and is given by

$$L_{230\ GHz,ADAF} \sim 2.5 \times 10^{38} m_7^{8/5} \dot{m}_{-3}^{6/5}\ erg\ s^{-1}, \quad (1)$$

where m_7 is the black hole mass in units of $10^7 M_\odot$ and $\dot{m}_{-3} = \dot{m}/10^{-3}$, where $\dot{m}$ is the accretion in units of Eddington rate. Using $m_7 = 5$ (Neumayer 2010) and $\dot{m}_{-3} = 0.2$ (Evans et al. 2004), the 230 GHz ADAF luminosity for Cen A is $\sim 5 \times 10^{38}$ erg s^{-1}, which is significantly lower than the observed 230 GHz radio luminosity. This implies that the ADAF component has a negligible contribution to the observed radio luminosity of the source.

Jet luminosity, in cases where it is mainly powered by black hole accretion, can be estimated using Equation (9) in Janssen

et al. (2021):

$$P_{jet} = 2.2 \times 10^{43} f(a_*) \left(\frac{\phi}{15}\right)^2 \left(\frac{\dot{M}}{10^{-6} \dot{M}_{Edd}}\right)$$

$$\times \quad \left(\frac{M}{6.2 \times 10^9 M_\odot}\right) erg\ s^{-1}, \quad (2)$$

where $0 \leqslant a_* \leqslant 1$ is the normalized black hole spin, $1 \leqslant \phi \leqslant 15$ is the normalized magnetic flux at the black hole event horizon, $f(a_*) \approx a_*^2 (1 + \sqrt{(1 - a_*^2)})^{-2}$ (for $a_* < 0.95$), $\dot{M} = 2 \times 10^{-4}$ $\dot{M}_{edd}$, and $M = 5 \times 10^7 M_\odot$. For $a_* \leqslant 0.2$ and $\phi \leqslant 1$, we have a marginally low jet power of $P_{jet} \leqslant \times 10^{39}$ erg s^{-1}. Slightly larger values of $a_* = 0.3$ and $\phi = 2$ give $P_{jet} \sim 1.5 \times 10^{40}$ erg s^{-1}, which well explains the observed radio luminosity.

Both the ADAF and jet models predict a strong correlation between the radio and X-ray flux variations. However, the ADAF models predict a very characteristic spectrum with a slope of $1/3$ in the radio regime (Mahadevan 1997). The observed radio spectrum of the source has a slope of $\sim$0.7 below the turnover frequency (around 5 to 20 GHz). A slightly steeper spectrum, with a slope of 0.8, is observed at higher frequencies (Israel et al. 2008). This implies that the observed radio spectrum of the source is not consistent with the ADAF model. Moreover, the shape of the hard X-ray spectrum in the ADAF models is thermal bremsstrahlung, not a power law. For low-luminosity AGNs (accreting close to $m_{critical} = 0.003$ to 0.02; Narayan 1996; Mahadevan 1997), the X-ray spectrum is very hard ($\Gamma \sim 0.7$). The power-law spectrum of Cen A, with Γ varying between 1.7 and 2, rules out the ADAF models. Another factor that argues in favor of the jet-based origin of the hard X-ray emission is the steepening of the X-ray spectrum as the source gets brighter. The ADAF models predict harder-when-brighter behavior (Esin et al. 1997). As discussed in Section 2.1, the spectrum gets steeper while the source gets brighter.

4. Conclusions

We present a thorough analysis of the hard X-ray emission from Cen A using 13 yr (2004 December–2017 December) of Swift/BAT observations. Prominent photon flux variations were detected during this period, and the variations are consistent with a red-noise process of slope -1.3. The source spectral variations were rather moderate until the end of 2012; a steeper-while-brighter trend was observed afterward. We found a significant correlation between the hard X-ray and 230 GHz

flux variations with no time lag, indicating the cospatiality of their emitting sites.

Previous spectral analysis confirms that the hard X-ray emission of the source is confined within the core, and is produced either via Comptonization in an ADAF flow or at the base of the inner jet (Fürst et al. 2016). The study could not disentangle the two. However, the variability analysis and the broadband spectral energy distribution studies of the source, using decade-long Rossi X-Ray Timing Explorer observations, favored the jet-based origin of the hard X-ray emission (Rothschild et al. 2011). Using a comprehensive analysis of the hard X-ray emission, and its correlation with the 230 GHz observations, we probe the hard-X-ray-emitting site in Cen A. The following arguments rule out the ADAF models: (1) the observed 230 GHz luminosity is significantly higher than $L_{230\,GHz,\,ADAF}$; (2) the radio spectral slope ($\sim$0.7–0.8) contradicts the characteristic slope of $1/3$ predicted by the ADAF models; (3) the power-law X-ray spectral shape; and (4) the softer-when-brighter behavior of the hard X-ray spectra. The study confirms the jet-based origin of the hard X-ray emission in the source.

ORCID iDs

B. Rani ⓘ https://orcid.org/0000-0001-5711-084X
S. A. Mundo ⓘ https://orcid.org/0000-0002-4504-3149
R. Mushotzky ⓘ https://orcid.org/0000-0002-7962-5446
M. A. Gurwell ⓘ https://orcid.org/0000-0003-0685-3621
J. Y. Kim ⓘ https://orcid.org/0000-0001-8229-7183

References

Abdo, A. A., Ackermann, M., Ajello, M., et al. 2010, Sci, 328, 725
Aharonian, F., Akhperjanian, A. G., Anton, G., et al. 2009, ApJL, 695, L40
Algaba, J.-C., Lee, S.-S., Kim, D.-W., et al. 2018, ApJ, 852, 30
Arnaud, K. A. 1996, in ASP Conf. Ser. 101, Astronomical Data Analysis Software and Systems V, ed. G. H. Jacoby & J. Barnes (San Francisco, CA: ASP), 17
Baek, J., Chung, A., Schawinski, K., et al. 2019, MNRAS, 488, 4317
Baity, W. A., Rothschild, R. E., Lingenfelter, R. E., et al. 1981, ApJ, 244, 429
Beckmann, V., Jean, P., Lubiński, P., Soldi, S., & Terrier, R. 2011, A&A, 531, A70
Burke, M. J., Jourdain, E., Roques, J.-P., & Evans, D. A. 2014, ApJ, 787, 50
Chatterjee, R., Marscher, A. P., Jorstad, S. G., et al. 2009, ApJ, 704, 1689
Chatterjee, R., Marscher, A. P., Jorstad, S. G., et al. 2011, ApJ, 734, 43
Chidiac, C., Rani, B., Krichbaum, T. P., et al. 2016, A&A, 590, A61
Done, C., & Gierliński, M. 2005, MNRAS, 364, 208
Edelson, R. A., & Krolik, J. H. 1988, ApJ, 333, 646
Esin, A. A., McClintock, J. E., & Narayan, R. 1997, ApJ, 489, 865
Evans, D. A., Kraft, R. P., Worrall, D. M., et al. 2004, ApJ, 612, 786
Fanaroff, B. L., & Riley, J. M. 1974, MNRAS, 167, 31P
Fukazawa, Y., Hiragi, K., Yamazaki, S., et al. 2011, ApJ, 743, 124
Fürst, F., Müller, C., Madsen, K. K., et al. 2016, ApJ, 819, 150
Gurwell, M. A., Peck, A. B., Hostler, S. R., Darrah, M. R., & Katz, C. A. 2007, in ASP Conference Ser. 375, From Z-Machines to ALMA: (Sub) Millimeter Spectroscopy of Galaxies, ed. A. J. Baker et al. (San Francisco, CA: ASP), 234
H.E.S.S. Collaboration, Abdalla, H., Adam, R., et al. 2020, Natur, 582, 356
Hardcastle, M. J., Worrall, D. M., Kraft, R. P., et al. 2003, ApJ, 593, 169
Harris, G. L. H., Rejkuba, M., & Harris, W. E. 2010, PASA, 27, 457
Hinkle, J. T., & Mushotzky, R. 2021, MNRAS, 506, 4960
Israel, F. P., Raban, D., Booth, R. S., & Rantakyrö, F. T. 2008, A&A, 483, 741
Janssen, M., Falcke, H., Kadler, M., et al. 2021, NatAs, 5, 1017
Kraft, R. P., Forman, W. R., Jones, C., et al. 2002, ApJ, 569, 54
Krimm, H. A., Holland, S. T., Corbet, R. H. D., et al. 2013, ApJS, 209, 14
Lohfink, A. M., Reynolds, C. S., Jorstad, S. G., et al. 2013, ApJ, 772, 83
Mahadevan, R. 1997, ApJ, 477, 585
Markowitz, A., Edelson, R., Vaughan, S., et al. 2003, ApJ, 593, 96
Markowitz, A., Takahashi, T., Watanabe, S., et al. 2007, ApJ, 665, 209
Marscher, A. P., Jorstad, S. G., Williamson, K. E., et al. 2018, ApJ, 867, 128
McHardy, I. M., Papadakis, I. E., Uttley, P., Page, M. J., & Mason, K. O. 2004, MNRAS, 348, 783
Müller, C., Kadler, M., Ojha, R., et al. 2014, A&A, 569, A115
Narayan, R. 1996, ApJ, 462, 136
Neumayer, N. 2010, PASA, 27, 449
Papadakis, I. E. 2004, MNRAS, 348, 207
Rani, B., Krichbaum, T. P., Marscher, A. P., et al. 2014, A&A, 571, L2
Rothschild, R. E., Markowitz, A., Rivers, E., et al. 2011, ApJ, 733, 23
Rothschild, R. E., Wilms, J., Tomsick, J., et al. 2006, ApJ, 641, 801
Shimizu, T. T., & Mushotzky, R. F. 2013, ApJ, 770, 60
Vaughan, S., Edelson, R., Warwick, R. S., & Uttley, P. 2003, MNRAS, 345, 1271
Vaughan, S., Fabian, A. C., & Iwasawa, K. 2005, Ap&SS, 300, 119
Worrall, D. M., Birkinshaw, M., Kraft, R. P., et al. 2008, ApJL, 673, L135
Wykes, S., Hardcastle, M. J., & Croston, J. H. 2015, MNRAS, 454, 3277
Yi, I., & Boughn, S. P. 1999, ApJ, 515, 576